Original

Blawert, C.; Karpushenkov, S.A.; Serdechnova, M.; Karpushenkava, L.S.; Zheludkevich, M.L.:

Plasma electrolytic oxidation of zinc alloy in a phosphate-aluminate electrolyte.

In: Applied Surface Science. Vol. 505 (2020) 144552.

First published online by Elsevier: 06.11.2019

https://dx.doi.org/10.1016/j.apsusc.2019.144552

Applied Surface Science 505 (2020) 144552

Contents lists available at ScienceDirect

Applied Surface Science

journal homepage: www.elsevier.com/locate/apsusc

Full Length Article

Plasma electrolytic oxidation of zinc alloy in a phosphate-aluminate electrolyte

C. Blawert[a], S.A. Karpushenkov[b], M. Serdechnova[a,*], L.S. Karpushenkava[b], M.L. Zheludkevich[a,c]

[a] Institute of Materials Research, Helmholtz-Zentrum Geesthacht, Max-Planck-Straße 1, 21502 Geesthacht, Germany
[b] Belarusian State University, Faculty of Chemistry, Nezavisimosti Avenue 4, 220030 Minsk, Belarus
[c] Institute for Materials Science, Faculty of Engineering, University of Kiel, Kaiserstraße 2, 24143 Kiel, Germany

ARTICLE INFO

Keywords:
Zinc
Plasma electrolytic oxidation
Phosphate-aluminate electrolyte
Optical emission spectroscopy
$ZnAl_2O_4$
ZnO

ABSTRACT

In the frame of this work, plasma electrolytic oxidation of a zinc alloy was performed in a phosphate-aluminate electrolyte as a first approach. Phase composition and microstructure of the formed PEO coating was analysed as a function of treatment time and applied current density. The coatings are mainly composed out of $ZnAl_2O_4$ and ZnO with some smaller amounts of $AlPO_4$ and $Zn_2P_2O_7$. The coating formation starts with ZnO at lower discharge energies and changes to the reactive formation of $ZnAl_2O_4$ when the discharge energy is increasing. The phase composition is only influenced by the final voltage and not by the current density. Latter is only determining the growth rate of the coating. However, stresses in the coatings are high and the layers are cracked and seems to flake-off already during PEO processing, thus at longer treatment times the coating thickness is not increasing anymore. To prevent extensive flaking-off of the coating a constant voltage PEO "repair" mode was introduced partly successfully at the end of the treatment.

1. Introduction

Plasma electrolytic oxidation (PEO) is an advanced anodizing process that leads to the formation of ceramic-like coatings on the surface of many active metals [1–11]. Those coatings are formed on the metallic surfaces due to short-lived micro-discharges, which took place under high voltages in low-concentrated, environmentally friendly electrolytes [12–14]. The oxide layers developed by PEO method are usually hard and well adherent to the substrates, thus they provide effective corrosion and wear resistance [15–19].

Up to now, PEO treatments are well known for corrosion and wear protection of magnesium [20,21], aluminium [22,23] and titanium [24] based alloys but only limited number of studies are available for zinc-based substrates [25–27]. However, zinc is an industrially important engineering alloy and control of its corrosion and wear properties is necessary. The development of PEO processes can facilitate zinc application for a number of industrial needs, e.g.:

(1) Transport application, e.g. maritime application for controllable sacrificial protection [28,29] and automotive applications for corrosion and wear protection [30], etc.

(2) Environmental application in particular in photocatalysis, where PEO based coating can be used for poisonous pesticides/herbicides decomposition [31] since ZnO formed during the process, broadens the emission band in the visible region. As a result, triggered poisonous compounds can be simpler decomposed directly under sun irradiation.

(3) Bio-medical application for implants with a biocompatible porous surface. Zinc is currently considered for degradable implants and PEO coatings can contribute to control their degradation as already demonstrated for Mg implants [32].

(4) Battery applications as cathodes, since electrically rechargeable zinc-air batteries have gained great attention in recent years due to their capacity to provide high energy density. For example, *E. Iruin et al.* have demonstrated that for zinc-air batteries aqueous chloride-based electrolytes can be considered as a possible alternative to the traditional alkaline system [33].

In the frame of this work, plasma electrolytic oxidation of zinc alloy was performed in phosphate-aluminate electrolyte as a first approach with the idea to form spinel phase which has interesting properties in the sense of chemical and thermal stability, hardness, catalytic and photocatalytic activity. Phase composition and microstructure of the formed PEO coating was analysed as function of treatment time and applied current density in order to understand what type of coatings are growing under the different conditions and to get an idea for which of the possible applications mentioned above the coatings can be used.

* Corresponding author. Tel.: +49 4152 87 1907; fax: +49 4152 87 1960.
E-mail address: maria.serdechnova@hzg.de (M. Serdechnova).

https://doi.org/10.1016/j.apsusc.2019.144552
Received 6 September 2019; Received in revised form 25 October 2019; Accepted 30 October 2019
Available online 06 November 2019

2. Experimental

Following materials and chemicals were used for electrolyte preparation and PEO synthesis in the frame of this work: potassium hydroxide (KOH, > 99%, Sigma-Aldrich Chemie GmbH, Germany), trisodium phosphate, sodium aluminate. Deionized water was used as a solvent. Zinc alloy sheet (Z1, according to EN988, VMZinc) with a nominal composition of [wt.%]: 0.08–1.00% Cu, 0.06–0.20% Ti, ≤0.015% Al and Zn balance (specimens dimensions of 20 * 25 * 1 mm) was used. Specimens were ground with 2500 grit emery paper and cleaned with ethanol before PEO treatment.

PEO processing was performed using a pulsed DC power supply under a constant voltage limit of 450 V and with a pulse ratio equal to t_{on}: t_{off} = 1 ms: 9 ms. The aqueous electrolyte (1 g L^{-1} KOH, 8 g L^{-1} Na_3PO_4 and 12 g L^{-1} $NaAlO_2$) was continuously stirred during the treatment process and kept at 20 ± 2 °C using a water cooling system. After the PEO treatment, the specimens were rinsed with deionized water and dried under air. Four different current densities (75, 100, 125 and 150 mA/cm^2) and three different treatment times (3, 6 and 12 min) were investigated.

Optical emission spectroscopy (OES) study was performed with a PLASUS Emicon system in order to determine the emission from the discharges during PEO layer formation under the different current densities. Low-resolution survey spectra were collected with a spectral resolution of ~ 1.5 nm (Δλ FWHM) for a period of 12 min in the range of 180–880 nm. Each individual spectrum was recorded for 500 ms (averaging over 50 pulses) every 10 s during the PEO treatment. The intensities of the main emission lines (Na, Zn, H, K) were monitored.

Surface morphology and cross-section observations of formed PEO coatings on zinc as a function of time and current densities were examined using *Tescan Vega3 SB* scanning electron microscope (SEM). In order to overcome the problem of surface charging during the SEM analysis, gold sputtering was performed prior to the SEM analysis in order to improve surface conductivity. The samples for cross-section investigations were prepared by grinding of resin embedded samples using 500, 800, 1200 and 2500 grit silicon carbide (SiC) paper, with a final polishing using diamond particles (1 µm). After the polishing, samples were rinsed with deionized water and dried under compressed air.

Phase compositions of the PEO-coatings as function of time and current densities were characterized using Bruker D8 Advances XRD at room temperature. Ni-filtered Cu Kα radiation was used. Following settings were applied during the measurements: 0.02° step size, 2 s dwell time, 3° glancing angle, and sample rotation rate – 20 s^{-1}. In order to estimate the amount and ratio of the formed phases during the PEO treatment, the normalization of XRD diffraction peaks was performed using the strongest $ZnAl_2O_4$ peak (3 1 1) as a reference for each diffraction measurements. In the case of ZnO phase, (0 0 2) peak was used for initial normalization, since this peak is not overlapping with other peaks present in the collected patterns (spinel and zinc substrate in our case). However, the presented normalized results are corrected using the standard ratio between (0 0 2) and (1 0 1) peaks (I_{002} : I_{101} = 24.2:100) in order to estimate the relative amount of ZnO phase in the coating.

3. Results

3.1. Voltage evolution and current density variation

The PEO process was operated under voltage and current control, which means that in the beginning the full pre-selected current density was applied until the pre-set voltage limit of 450 V was reached. After that the voltage is maintained and with increasing layer thickness or density (resistance), the current density is dropping. Fig. 1 shows the voltage (a) and current density (b) as a function of PEO processing time for the four selected current densities (75, 100, 125 and 150 mA/cm^2) and 450 V voltage limitation. The four different current densities were chosen to check if the growth rate influences the porosity and the stresses in the coatings.

The two stages of the PEO process can be clearly distinguished in these graphs. The main idea behind this concept was to grow the layers under galvanostatic (constant current) mode and heal them under potentiostatic (constant voltage) mode (Table 1). The curves are typical voltage- and current-time curves for PEO processing. The voltage is ramping faster if the current density is higher indicating that the coating is growing faster (thicker and/or denser layer) and the voltage has to be increased to maintain the pre-selected current density. Once the voltage limit is reached the coating is continuing to grow and the current is dropping because of this. This stage is considered as a kind of repair stage of the coating and it is reached after 143, 190, 287 and 479 s of treatment time depending on the current density selected (Table 1 and Fig. 1). Discharges occur only in the weakest locations of the coating healing the defects [34,35]. The drop of current is a good indicator of this repair and for the two highest current densities the repair is finished after 12 min of treatment. In this case, the current density is below 5 mA/cm^2 and only sporadic discharges are visible indicating that the coating thickness and/or density are so high that the applied voltage of 450 V is almost not able to generate electrical break down of the coating anymore. Because of the shorter repair stage (longer ramp-up time and same total treatment time), the repair is not fully done for the 100 and 75 mA/cm^2 specimen and the current density at the end of the 12 min treatments are still 7.5 and 11.5 mA/cm^2, respectively. For all the other shorter treatment times (even at the highest current density) the repair is not fully done as well, according to the current-time curves, presented in Fig. 1 and given in Table 1.

The coating formation, morphology and phase composition during PEO processing depends strongly on the discharges, which are changing with treatment time [36,37]. In the beginning they are small and their lifetime is short and closer to the end of the process they became larger and more stationary. With this change of mobility and size also the colour of the sparks is changing (see Table 2 for more information). According to the colour of the discharges, four different types of discharges are visible and can be also followed by OES measurements (Fig. 2). However, regardless of the chosen current densities, it was observed, that the average nature of those PEO sparks depends mainly on the voltage applied to the sample, but not on the current density (Fig. 2 a and b). Of course the voltage is reached at different treatment times with different current densities. The different voltage regions according to the appearance of the different sparks are marked in Fig. 1 as well. Optical emission spectra obtained for the samples under an applied current density of 100 mA/cm^2 and 150 mA/cm^2 during the PEO treatment are presented in Fig. 2 and a description of the visual appearance of the sparks as a function of applied voltage is given in Table 2. At the same voltage the spectra do not reveal large differences.

It can be seen from Fig. 2, that only a broad halo in the visible zone (450 – 650 nm) can be detected for the treatments below 300 V. Visually it appears as white shining of the entire sample up to 250 V, when the first white discharges are starting without a sign of specific emission lines. This effect can be explained via the presence of free electrons in the plasma interacting with solid and/or liquid compounds (zinc substrate or electrolyte/ Bremsstrahlung) and is often attributed to the conventional oxidation stage and the oxygen production on the surface [38–40].

Starting from ca. 310 V, the strong line of sodium emission appears in the spectra. This emission is obviously responsible for the change of colour of the sparks into yellow-orange. With further increase of applied voltage (from around 340 V), emission lines of zinc became visible as well. They are obviously contributing to the visual impression that some sparks are purple. It should be noted that at this stage sparks with the different colours still co-exist at the surface. The white shining of the sample disappears when the treatment times get longer (more than 400 s) and large intensive orange, more stationary discharges (sodium)

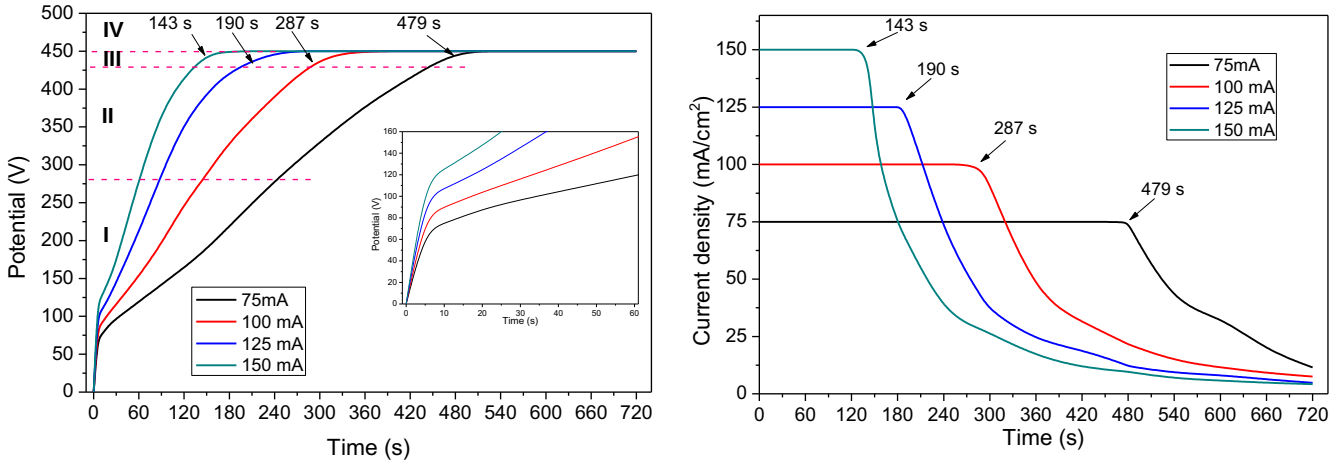

Fig. 1. Voltage (a) and current density (b) evolution as a function of PEO processing time.

Table 1
Voltage–current parameters at the end of PEO treatments.

Current density (mA cm^{-2})	final voltage (V) / final current density final (mA/cm^2)			CC → CV (sec)
	3 min	6 min	12 min	
75	219/75	378/75	450/11.5	479
100	331/100	450/42.5	450/7.5	287
125	424/125	450/23.2	450/4.8	190
150	450/74.4	450/16.5	450/4.2	143

and yellow short-living discharges are dominating on the surface. This can be explained, by initially solid zinc substrate being evaporated and subsequently being involved in the plasma formation. However, since formed PEO layer became thicker with time, the white shining, related to more classical anodising of the metal surface, could not be detected anymore [41,42]. Furthermore, it has to be considered that due to the constant voltage mode at the end of the treatment, the current density is going down and probably a reduced number of free electrons is available. Potassium emission may contribute to the more intense "orange" and zinc emission might be masked by it. Overall, Table 2 summarises the visually observable characteristics of the sparking depending on the applied voltage.

From the emission spectra it is also seen, that hydrogen (both H atom and H_2) is exited in the discharges during PEO processing if the discharge energy is higher at the end of the process. Surprisingly, oxygen (O, O_2 or OH) does not play an important role in the emission of the discharges and except Zn, there is no element involved in the discharges that finally forms the coating.

3.2. Surface and cross-sectional morphologies

The surface morphology shown in Fig. 3 clearly reveal that the produced coatings are highly stressed and do not have good adhesion to the surface and/or cohesion problems within the layers regardless of which current density is used. Even the thinnest layer after 3 min at 75 mA/cm^2 is already starting to peel-off. The adhesion/cohesion remains weak as long as the current density remains constant. Due to this fact we have selected a treatment concept that growths the layer under constant current density and tries to repair it under constant voltage mode (with continuously reduced current densities). Considering the obtained results, where the repair process has started (in the case of 100, 125, 150 mA/cm^2 with treatment times equal or longer than 6 min and in the case of 75 mA/cm^2 for 12 min treatment), the "repair" concept seems to work to a certain degree. Due to higher energy discharges (indicated by larger pore sizes) but quite low amount, the surface seems to be sintered much better and the adhesion seems to be improved while stresses are released.

Problems with adhesion or cohesion are also visible in the cross-sections of the coatings (Fig. 4). During specimen preparation for some conditions, the coatings are fully delaminated along the interface of Zn substrate/coating. The process of flaking-off is captured in some of the cross-sections (e.g. Fig. 4-k) with some of the coating tilted and lifted-off from the surface. The new coating is already grown underneath it.

Table 2
Visual observation during PEO treatments.

	Voltage	Visual observations
I	0–240 V	No visible sparking is observed, however white shining of the sample was already detected using OES measurements at least at 110 V
	250 V	The very first small white sparks appear at the edges of the sample and can be detected visually
	260 V	The small white short-living sparks spread over the entire surface of the oxidizing sample
II	280 V	Sparks at the edges of the sample become larger and get more white-purple in colour, first yellow/orange sparks became visible as well
	300 V	The small white sparks and enlarged white-purplish sparks are observed over the entire surface of the oxidizing sample as well as orange sparks enlarge.
III	430 V	The main sparks became orange and live-time is increasing.
	440 V	Larger zones of yellow sparks appear at the edges of the sample. White shining disappear.
IV	450 V	Over the entire surface, there are small sparks of yellow and large stationary sparks of orange colour. Orange also became more intensive in colour. Following the increase of coating thickness (oxidation time), the number of sparks decreases and, after ca. 10 min of PEO treatment, only single large sparks and a low number of small sparks are visible on the surface.

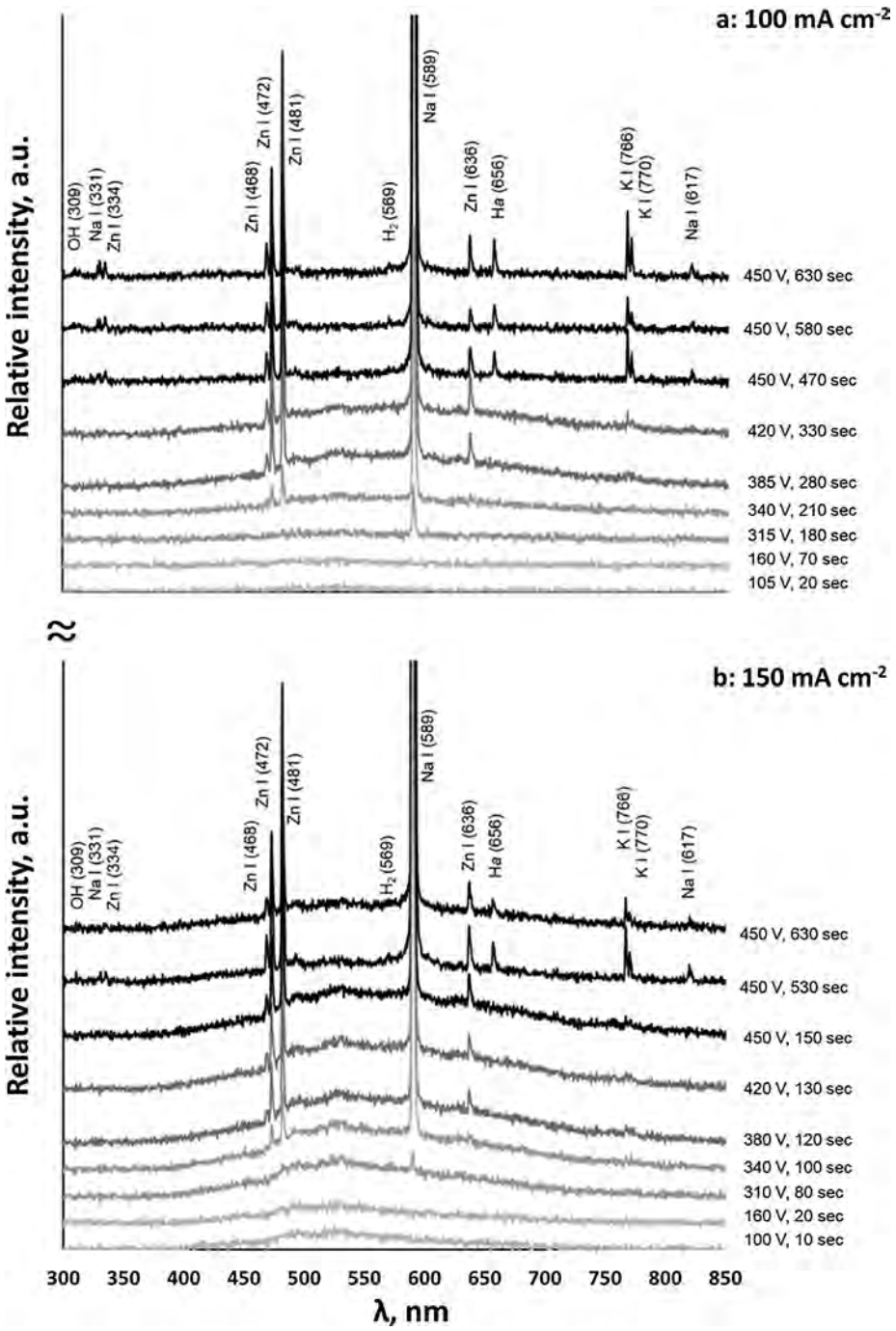

Fig. 2. Optical emission spectra obtained during PEO treatment under 100 mA/cm^2 (a) and 150 mA/cm^2 (b) current densities.

This is one of the reasons, why the coatings are quite rough on the surface and thickness variation is quite high (Table 3). Nevertheless, the expected increase in the coating thickness with increasing current density is visible after 3 min treatment. The average coating growth rates estimated from the coating thicknesses are 1 μm/min, 3 μm/min, 5 μm/min and 7 μm/min when increasing the current density stepwise from 75 to 150 mA/cm^2. However, with the increasing current density, the influence of treatment time on the increase of coating thicknesses is reduced because the voltage limit of 450 V is reached faster and the process changed from constant current to constant voltage mode with continuously decreasing current density and growth rate. Thus, more time is spent to repair the coatings rather than growing them thicker. For the treatment time of 12 min or the highest current densities, the thickness of PEO coatings stays almost constant around 20 μm and does not depend on treatment time anymore. However, the combination of highest current density and longest treatment time allows the current density to drop to almost zero at the end of the process and the relative thickness variation is the smallest (Tables 1 and 3). This observation agrees well with the idea of coating flacking-off due to the internal stresses and its repair under milder PEO conditions.

3.3. Elemental and phase composition of the coatings

The coatings are mainly composed of $ZnAl_2O_4$ with some content of ZnO and even smaller amounts of $AlPO_4$ and $Zn_2P_2O_7$ (Fig. 5). ZnO is present in a higher amount when the combination of treatment time and current density was not sufficient to reach the final 450 V (e.g. 3 min 75 mA/cm^2, see Table 1). As soon as the final voltage of 450 V

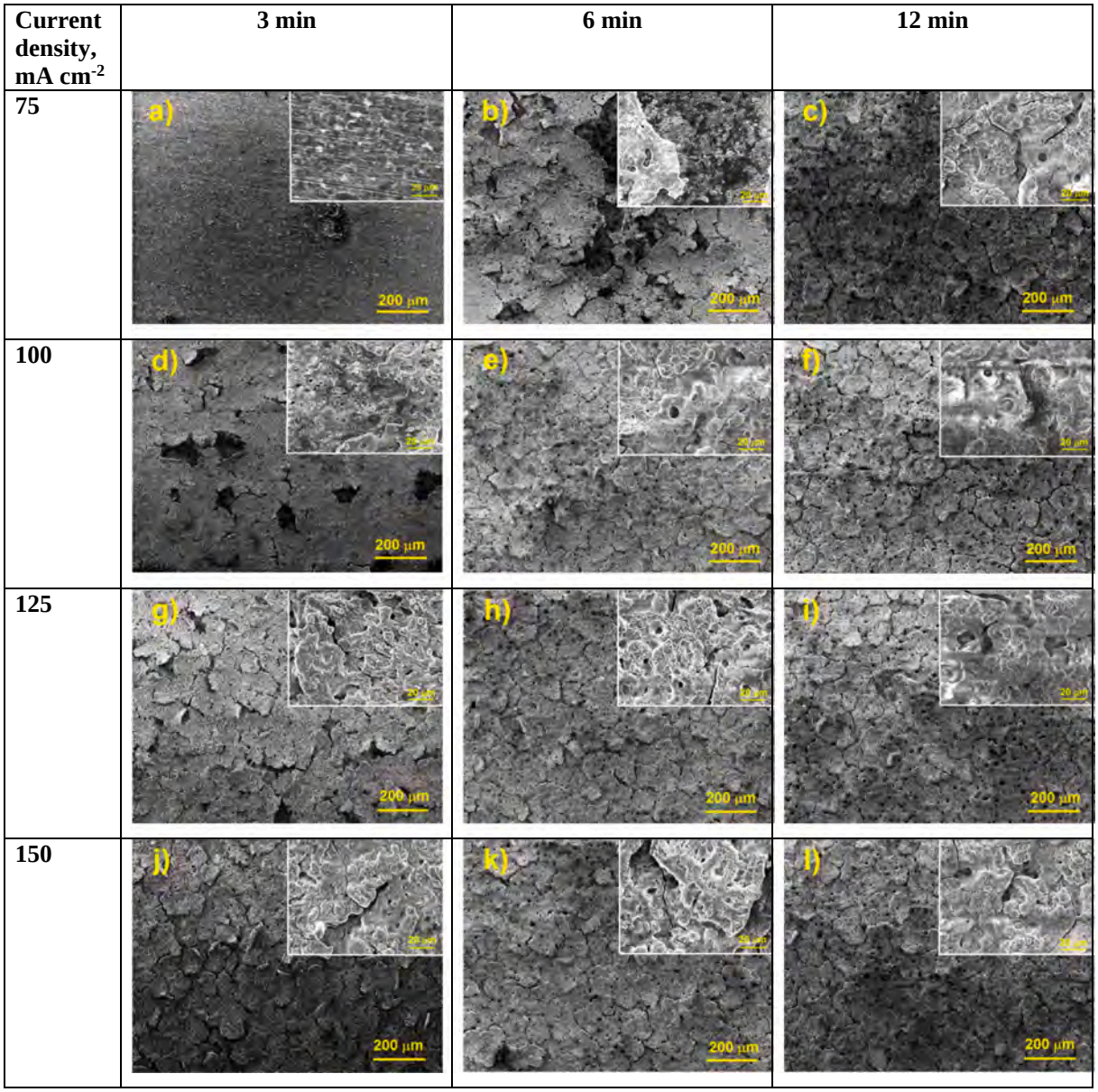

Fig. 3. Surface morphology as a function of current density and treatment time.

was reached the main coating phase was $ZnAl_2O_4$. To eliminate the influence of surface roughness or small tilts of XRD specimens during the measurements on peak intensities all important diffraction peaks were normalised according to the intensity of the respective strongest $ZnAl_2O_4$ peak (Table 4). The normalised Zn intensity is a good indicator for the coating thickness as the signal is coming from the substrate and is reduced with increasing coating thickness. For the shortest treatment time of 3 min a clear effect of increasing current density on coating thickness is visible reducing the normalised Zn intensity (7.65–0.56–0.10–0.05 respectively). At the lowest current density, there is still a small effect of treatment time visible, but all other parameter combinations do result obviously in similar coating thicknesses. This is in good agreement with the thickness measurements performed on the cross-sections.

Similar observations are done when the phase composition of the coating is considered by the intensity ratios of $ZnO/ZnAl_2O_4$, $AlPO_4/ZnAl_2O_4$, and $Zn_2P_2O_7/ZnAl_2O_4$, respectively. Assuming that the normalised intensity is identical to the phase fraction of the specific phases, the amount of ZnO in the coating is higher than $Zn_2P_2O_7$ and later is still higher than $AlPO_4$. All three are lower than $ZnAl_2O_4$ (except for 3 min 75 mA/cm^2). The trend of changes in coating composition with processing conditions is similar to the change of coating thickness (Table 4). At shorter treatment times the amount of all three phases is reduced with increasing current density and there is only a small influence of treatment time visible at the lowest current density. The main reduction occurs between 3 and 6 min and then almost no change is visible suggesting that the coating compositions are mainly depending on the final voltage and not that much on the treatment time at a final voltage (Tables 1 and 4). However, those treatments were 400 V were not reached are marked with an asterisk (*) in Table 4 and it is quite obvious that under those conditions the phase fractions of ZnO, $Zn_2P_2O_7$ and $AlPO_4$ in the coating are higher than under those conditions where it was reached. It seems as if at voltages above 400 V the reactive formation of $ZnAl_2O_4$ is further improved or that the main location of formation of the other phases is at the interface becoming less visible if the coating thickness is increased.

The composition of the near surface region (measured by EDS from the top surface) is shown in Table 5. The main coating forming elements in decreasing order are oxygen, zinc, aluminium, carbon, sodium and phosphor. The oxygen level is quite constant (44 – 45 at.%) except for

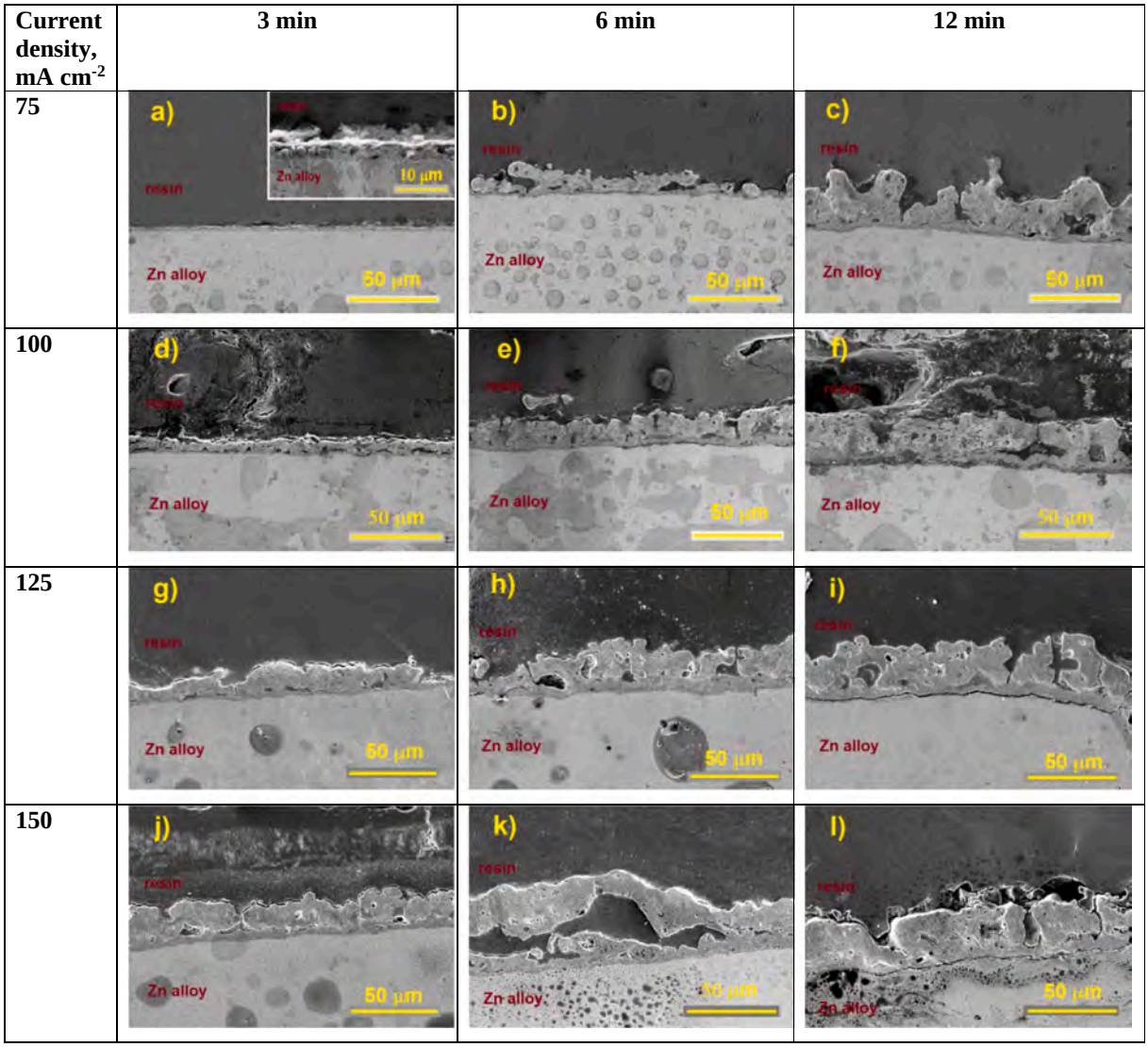

Fig. 4. Cross-sections of the coatings obtained under the different parameter combinations.

Table 3
Average thicknesses (µm) of the obtained coatings as a function of treatment time and applied current densities. Standard deviations are also indicated.

Current density	Time	3 min	6 min	12 min
75 mA cm^{-2}		3 ± 1	10 ± 5	15 ± 10
100 mA cm^{-2}		10 ± 5	15 ± 10	20 ± 10
125 mA cm^{-2}		15 ± 10	20 ± 10	20 ± 10
150 mA cm^{-2}		20 ± 10	20 ± 10	25 ± 5

the shortest treatment time with the lowest current density where the oxygen content is around 53.5 at.%. This may indicate that there is still a higher fraction of conversion products ($AlPO_4$ and $Zn_2P_2O_7$ phosphates as seen by XRD) explaining the higher oxygen content. The overall oxygen content is too low to balance all possible metal and phosphor atoms considering the phases identified by XRD and those, which are likely from the elemental analysis e.g. some carbonates (C) and Na_3PO_4/Na_2O. However, it is not unusual for PEO coatings that the oxygen level is lower than necessary to fully explain the observed phase formation [43,44]. Nevertheless, considering only the three main elements Zn, Al and O, the measured concentrations are reasonable to explain the formation of the main coating phase $ZnAl_2O_4$ by a reactive phase formation between ZnO and Al_2O_3. Interestingly, the ratio of Zn and Al is not constant and at short treatment times the Zn content is higher decreasing with increasing treatment time (from 20 ± 1 to 15 ± 1 at.%). The aluminium content shows exactly the opposite trend increasing from 18 ± 1 to 21 ± 1 at.%. The trend is shown in Fig. 6. A possible explanation for this is the changing availability of Zn and Al with increasing coating thickness as Zn is mainly coming from the substrate and aluminium from the electrolyte.

4. Discussion

The main intention of the present study was to see if it is possible to synthesize $ZnAl_2O_4$ spinel phase on the surface of a Zn alloy via PEO processing in an aluminate-phosphate based electrolyte. It was successfully demonstrated that coatings with a predominant composition of $ZnAl_2O_4$ and minor contents of ZnO, ZnP_2O_7 and $AlPO_4$ can be produced. The spinel phase was already dominating when a voltage higher than 300 V was reached, thus the phase formation is mainly controlled by the applied voltage. The phase formation was quite independent of the treatment time (as long as the needed voltage was reached) and the current density. Latter determines only how quick the coatings are growing and how quick the intended voltage of 450 V is reached.

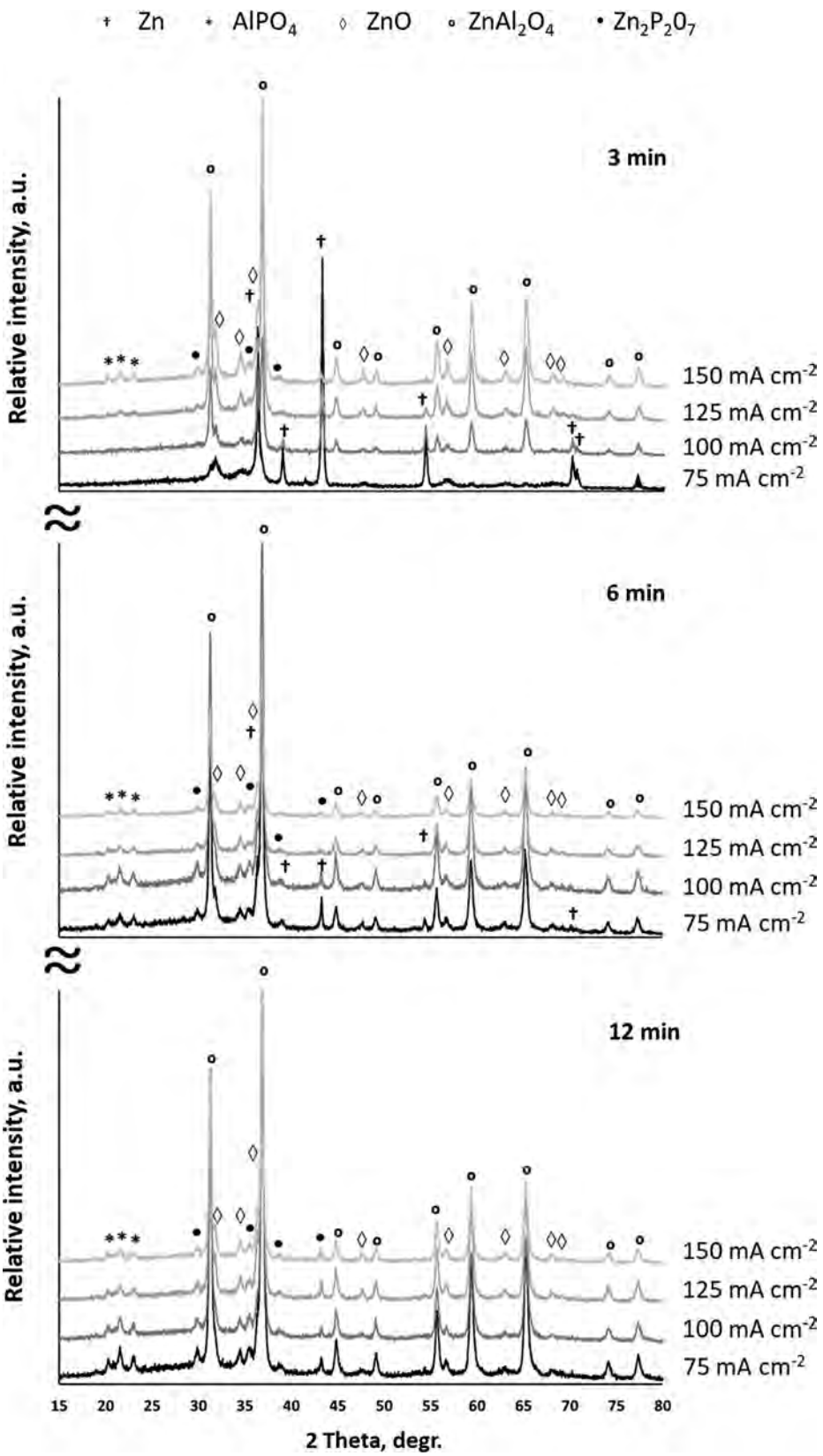

Fig. 5. XRD patterns of obtained PEO coatings as a function of current density and treatment time.

Looking at the OES results, only Zn and OH emission lines from the coating forming elements or molecules are visible and present in the discharges in a form of linear spectra. There seems to be only a limited number of reactions in the plasma to form the coating compounds. However, the continuous emission may indicate that there are additional interaction between the gas phase and melted/solid metal/oxide surfaces [38–40].

The phase formation during PEO processing involving the

Table 4
Normalized XRD peaks intensities for phase identification, extracted from Fig. 5.

	Current density, mA cm^{-2}	2 theta	Lattice plane		3 min	6 min	12 min
Zn	**75**	43.24	(1 0 1)	Abs.	2074*	308*	157
				Norm.	7.65*	0.15*	0.05
	100	43.24	(1 0 1)	Abs.	602*	157	140
				Norm.	0.56*	0.06	0.06
	125	43.24	(1 0 1)	Abs.	206	72	182
				Norm.	0.10	0.05	0.07
	150	43.24	(1 0 1)	Abs.	119	57	99
				Norm.	0.05	0.05	0.05
ZnO	**75**	34.42	(0 0 2)	Abs.	178*	200*	234
				Norm.	3.36	0.54	0.43
	100	34.42	(0 0 2)	Abs.	145*	227	208
				Norm.	0.84	0.46	0.51
	125	34.42	(0 0 2)	Abs.	261	131	213
				Norm.	0.77	0.47	0.48
	150	34.42	(0 0 2)	Abs.	317	115	180
				Norm.	0.72	0.44	0.38
$ZnAl_2O_4$	**75**	36.82	(3 1 1)	Abs.	212*	1489*	2188
				Norm.	1*	1*	1
	100	36.82	(3 1 1)	Abs.	693*	1973	1635
				Norm.	1*	1	1
	125	36.82	(3 1 1)	Abs.	1361	1119	1765
				Norm.	1	1	1
	150	36.82	(3 1 1)	Abs.	1766	780	1395
				Norm.	1	1	1
$AlPO_4$	**75**	20.30	(2 2 0)	Abs.	67*	139*	169
				Norm.	0.25*	0.07*	0.06
	100	20.30	(2 2 0)	Abs.	82*	176	145
				Norm.	0.08*	0.06	0.06
	125	20.30	(2 2 0)	Abs.	82	76	102
				Norm.	0.04	0.05	0.04
	150	20.30	(2 2 0)	Abs.	128	57	98
				Norm.	0.05	0.05	0.05
$Zn_2P_2O_7$	**75**	30.04	(2 1 1)	Abs.	126*	197*	234
				Norm.	0.46*	0.10*	0.08
	100	30.04	(2 1 1)	Abs.	137*	216	153
				Norm.	0.13*	0.08	0.07
	125	30.04	(2 1 1)	Abs.	163	97	144
				Norm.	0.08	0.06	0.06
	150	30.04	(2 1 1)	Abs.	204	56	112
				Norm.	0.08	0.05	0.06

Table 5
Composition (in at.%) of PEO coatings by EDS analysis of the top surface, average.

		Zn	Al	O	P	Na	K	Ti	C
75 mA cm^{-2}	**3 min**	23.37	10.08	53.46	3.68	3.21	0.07	0.04	6.09
	6 min	19.88	16.45	44.75	4.64	5.53	0.18	0.02	8.55
	12 min	15.69	21.31	45.38	3.76	6.67	0.17	0.01	7.01
100 mA cm^{-2}	**3 min**	19.95	16.91	44.54	4.60	5.20	0.16	0.02	8.62
	6 min	16.85	19.43	45.05	4.14	7.82	0.20	0.03	6.48
	12 min	15.81	20.76	44.94	3.65	6.51	0.18	0.02	8.13
125 mA cm^{-2}	**3 min**	21.05	17.85	44.08	4.11	5.92	0.17	0.02	6.80
	6 min	17.81	20.62	44.60	3.55	6.43	0.17	0.02	6.80
	12 min	14.12	21.48	45.76	3.94	6.48	0.17	0.03	8.02
150 mA cm^{-2}	**3 min**	18.97	19.19	44.68	3.82	6.14	0.19	0.02	6.99
	6 min	16.83	21.23	44.99	3.60	6.45	0.20	0.02	6.68
	12 min	15.74	22.08	45.44	3.71	6.31	0.17	0.02	6.53

discharges is still not fully understood and depends strongly on the HV pulse parameters, the electrolyte and the substrate. In the locations of the micro-discharges complex oxide formation mechanisms take place involving chemical, electrochemical, plasma-chemical, pressure and thermal activated processes involving gas, liquid and solid states of the metal/oxide surface and the electrolyte. In our case, most of the formation of the coating does obviously not happen directly in the plasma of the discharges as there are only Zn and OH emission lines from the coating forming elements or molecules visible. However, there is the continuous emission visible in the OES spectra, which may indicate that there are reactions and formation of oxides due to interactions of plasma and liquid/solid states as well [41,42]. This continuous emission is disappearing at the end of the treatment processes, which might be related to the fact that the current density is reduced and the number of discharges gets less and thus the overall emission intensity is going down. Nevertheless, direct reactions in the plasma to form the coating compounds seems to be not the main formation mechanism throughout the whole treatment period, since there is a clear dependence between the phase formation and the applied voltage. A threshold value of around 300 V (discharges start at 250 V) has to be exceed to stimulate spinel formation. Below 300 V the main phase is ZnO. It can be expected that the energy/temperature in any discharge (T_e: 4000–10,000 K [45]) is sufficient to form the mix-oxide (spinel) as the main coating component directly, but this does not happen at the lower discharge voltages. With the change of discharges and increasing energy in the discharges, the emission spectra is also changing, but apart from this 300 V threshold without any relation to the formed phases in the coating. However, thus it is more likely that phases are formed by thermal and galvanically stimulated chemical conversion processes, which are responsible for the deposition of phases on the surface also during the HV off-time. The energy provided by the discharges during the HV on-time is finally sintering them. The sintering step can include thermal decomposition, liquid phase formation and reactive sintering of phases. The sintering step takes place in/on the existing surface of the oxide, mixing the conversion products with the already existing oxides from previous discharges. Due to the complex formation processes, the short lifetime of the discharges and the quick quenching due to the electrolyte and bulk substrate close to room temperature not the full energy of the discharges is available for the sintering. Effective temperatures which can be reached as soon as the 300 V are exceeded seems to be around 1800 °C occurring locally in the oxide film (based on the observed phase formation).

In the present case, the following simplified steps of coating formation under the high energy discharges of the PEO process are suggested [Eqs. (1)–(5)]:

$$Zn \rightarrow Zn^{2+} + 2e^- \quad (1)$$

$$Zn^{2+} + 2OH^- \rightarrow Zn(OH)_2 \quad (2)$$

$$Zn(OH)_2 \rightarrow ZnO + H_2O \quad (3)$$

$$2AlO_2^- + H_2O \rightarrow Al_2O_3 + 2H_2O \quad (4)$$

$$Al_2O_3 + ZnO \rightarrow ZnAl_2O_4 \quad (5)$$

Under the anodic potential Zn dissolves (Eq. (1)) and reacts with hydroxide ions to $Zn(OH)_2$ (Eq. (2)). Due to the low solubility ($K_{SP} = 3 \times 10^{-17}$) it is redeposited as a conversion product on the surface of the Zn anode. Under the energy (heat) of the discharges, it is decomposed to ZnO and water (Eq. (3)). Also under the energy of the discharges AlO_2^- ions are reacting with water to aluminium oxide and hydroxide ions as a side product (Eq. (4)). The two oxides ZnO (T_{Melt} = 1975 °C) and Al_2O_3 (T_{Melt} = 2072 °C) are finally reacting to form the mixed oxide (spinel) $ZnAl_2O_4$. The mixed oxide has a lower melting point than the single oxides [46] and thus formation should be easier. In a ZnO rich surrounding that exists on the surface of the Zn anode, spinel should form at temperatures around 1739 °C. Considering the fact that there is no Al_2O_3 visible in the XRD pattern it is likely that the formed Al_2O_3 directly reacts with ZnO to the spinel $ZnAl_2O_4$.

It is quite obvious that the coating formation starts with ZnO at lower discharge energies as the thermal decomposition of $Zn(OH)_2$ does not need high temperatures (100–150 °C) [47] and changes to the reactive formation of $ZnAl_2O_4$ when the discharge energy is increasing. According to XRD results, at a final voltage of 219 V the coating is dominated by ZnO, but this is changing when the voltage is exceeding

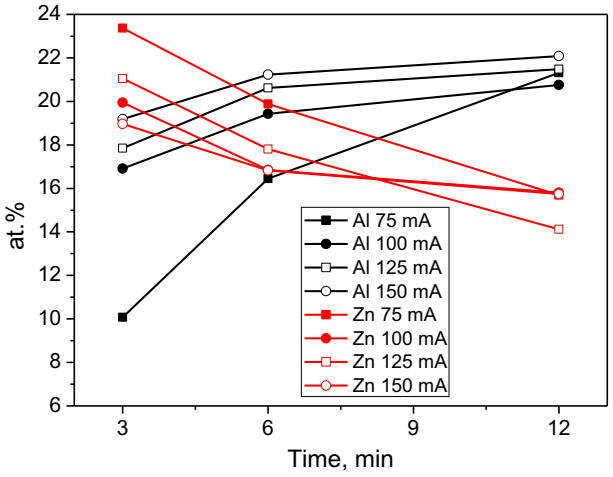

Fig. 6. Evolution of the content of Zn and Al in the coatings depending on PEO processing duration.

300 V and spinel is more dominant for the first time. However, at final voltages below 400 V the ZnO is still present at higher volume fraction especially when the treatment times are short. This finding is also supported by the elemental compositions (Table 5). There is always Zn (ZnO) in excess, not needed to balance the aluminium to form the spinel phase. At lower times and voltages, the amount of excess Zn is higher, suggesting that the phase formation depends also on the discharges and the mixing in the liquid phases, existing locally during the discharges. More discharge energy at longer treatment times seems to increases the volume of a liquid phase and eases the Al_2O_3 formation from the AlO_2^- and finally the reaction to spinel.

From the phase composition in correlation with the processing parameters it is clear that it is mainly influenced by the final voltage and not by the current density. At 450 V the coatings are mainly composed of $ZnAl_2O_4$ and ZnO (and smaller remains of $AlPO_4$ and $Zn_2P_2P_7$) and the phase fractions are quite constant. $AlPO_4$ and $Zn_2P_2O_7$ phases have higher phase fractions when the final voltage was not reached and more conversion products are still incorporated into the coating. At these lower voltages (around 300 V) and even at 219 V the reactive formation of spinel is already possible but less efficient (probably due to the required pre-reaction of aluminate to alumina, which needs most likely higher energy than the Zn hydroxide decomposition). Thus a larger amount of ZnO is formed without a reaction partner (Al_2O_3) and remains sintered as a main part of the coating.

Looking at the influence of current density, it is not influencing the phase composition much, but the growth rate of the coatings. Changing the current density from 75 to 150 mA/cm^2 increases the growth rate from 1 µm/min to 7 µm/min. However, the change of growth rate has no positive effect on the observed thickness-dependent adhesion/cohesion problems of the coatings. Stresses in the coatings seems to be high and the layers are cracked and flake-off already during PEO processing, thus at longer treatment times, the coating thickness is not increasing anymore. As soon as a thickness of around 15 ± 5 µm is reached the coatings start to flake-off. The Pilling Bedworth Ratio (PBR) for ZnO is 1.58 and for the $ZnAl_2O_4$ it is 1.45, thus the fit to the lattice of the Zn substrate should not be a problem. Actually, according to the PBR, it should be possible to grow dense and adhesive layers, but this is not the case, independently of the chosen speed to grow the layers. The appearance of the surface suggests that the cracking occurs already during the PEO process, thus it is most likely that differences in the thermal expansion might be the reason. At room temperature the Zn substrate, ZnO and $ZnAl_2O_4$ have expansion coefficients of $3{\cdot}10^{-5}$, $4.8{\cdot}10^{-5}$ and $7.1{\cdot}10^{-6}$, respectively [48–50]. Thus there is a bigger difference between substrate and coating, especially with the spinel phase. Furthermore, the spinel contracts with increasing temperature while the Zn and ZnO actually expand [51]. This different behaviour may explain the observed poor adhesion or cohesion caused by thermal-induced stresses. The different current densities were obviously not able to change the stresses and improve adhesion/cohesion.

To prevent extensive flaking-off of the coating a constant voltage PEO "repair" mode had to be introduced at the end of the treatment. Higher energy discharges at lower frequency were obviously able to increase the size of melt pools and reduce the cooling rate of the liquid phase. Thus stresses could be better released and the defects were healed out as the few late discharges (at current densities below 5 mA/cm^2) mainly in the weakest regions without causing new cracks. The successful proof of "repair" concept was visible in the surface morphologies of the specimens treated at higher current densities. With the fixed maximum total treatment time of 12 min, the repair was only fully finished for the two highest current densities and they show the best surface appearance after the treatment.

5. Conclusions and summary

Overall, in the frame of this study, it was demonstrated that

1) It is possible to grow $ZnAl_2O_4$ spinel rich layers on Zn alloy from aluminate phosphate-based alkaline electrolytes.
2) The coatings are composed mainly from $ZnAl_2O_4$ and ZnO. Minor amounts of phosphates ($Zn_2P_2O_7$ and $AlPO_4$) are also present. At lower final voltage the coating is mainly formed from ZnO and above 300 V the spinel phase is dominant.
3) The formed coatings are highly stressed and tend to flake-off if the coatings are growing too thick (more than 15 ± 1 µm).
4) A mixed constant current mode/constant voltage mode was successfully introduced to reduce the stresses and to obtain visually almost defect-free coatings (pores and some cracks still exist as usual for PEO coatings)
5) Due to the high content of $ZnAl_2O_4$ phase in the coating, they might be interesting for transport (corrosion and wear), biomedical (degradation control of degradable Zn implants) or environmental applications (photocatalytic waste water cleaning).

Declaration of Competing Interest

The authors declare that they have no known competing financial interests or personal relationships that could have appeared to influence the work reported in this paper.

Acknowledgements

This work was partially supported by FUNCOAT project ("Development and design of novel multiFUNctional PEO COATings") in frame of H2020-MSCA-RISE-2018, Grant Agreement N 823942.

References

[1] Gh. Barati Darband, M. Aliofkhazraei, P. Hamghalam, N. Valizade, Plasma electrolytic oxidation of magnesium and its alloys: Mechanism, properties and applications, J. Magnesium Alloys 5 (1) (2017) 74–132, https://doi.org/10.1016/j.jma.2017.02.004.
[2] M. Toorani, M. Aliofkhazraei, Review of electrochemical properties of hybrid coating systems on Mg with plasma electrolytic oxidation process as pretreatment, Surf. Interfaces 14 (2019) 262–295, https://doi.org/10.1016/j.surfin.2019.01.004.
[3] X. Lu, M. Mohedano, C. Blawert, E. Matykina, R. Arrabal, K.U. Kainer, M.L. Zheludkevich, Plasma electrolytic oxidation coatings with particle additions – A review, Surf. Coat. Technol. 307 (Part C) (2016) 1165–1182, https://doi.org/10.1016/j.surfcoat.2016.08.055.
[4] B.L. Jiang, Y.M. Wang, "5 - Plasma electrolytic oxidation treatment of aluminium and titanium alloys" Surface Engineering of Light Alloys: Aluminium, Magnesium and Titanium Alloys, Woodhead Publ. Ser. Metals Surf. Eng. (2010) 110–154, https://doi.org/10.1533/9781845699451.2.110.
[5] A. Lugovskoy, S. Lugovskoy, Production of hydroxyapatite layers on the plasma electrolytically oxidized surface of titanium alloys, Mater. Sci. Eng., C 43 (2014) 527–532, https://doi.org/10.1016/j.msec.2014.07.030.

[6] M. Serdechnova, S.A. Karpushenkov, L.S. Karpushenkava, M. Starykevich, M.G.S. Ferreira, T. Hack, M.H. Iuzviuk, I.A. Zobkalo, C. Blawert, M.L. Zheludkevich, The influence of PSA pre-anodization of AA2024 on PEO coating formation: composition, microstructure, corrosion, and wear behaviors, Materials 11 (2018) 2428, https://doi.org/10.3390/ma11122428.

[7] A. Bordbar-Khiabani, S. Ebrahimi, B. Yarmand, Plasma electrolytic oxidation of monocrystalline silicon using silicate electrolyte containing boric acid, Appl. Surf. Sci. 462 (2018) 913–922, https://doi.org/10.1016/j.apsusc.2018.08.155.

[8] S. Stojadinović, N. Tadić, R. Vasilić, Plasma electrolytic oxidation of hafnium, Int. J. Refract Metal Hard Mater. 69 (2017) 153–157, https://doi.org/10.1016/j.ijrmhm.2017.08.011.

[9] S.A. Karpushenkov, A.I. Kulak, G.L. Shchukin, A.L. Belanovich, Microplasma electrochemical deposition of aluminum oxide-polyethylene composite coatings on iron surface, Prot. Met. Phys. Chem 46 (4) (2010) 463–468, https://doi.org/10.1134/S207020511004012X.

[10] M. Sowa, A. Kazek-Kęsika, R.P. Socha, G. Dercz, J. Michalska, W. Simka, Modification of tantalum surface via plasma electrolytic oxidation in silicate solutions, Electrochim. Acta 114 (2013) 627–636, https://doi.org/10.1016/j.electacta.2013.10.047.

[11] S.A. Karpushenkov, G.L. Shchukin, A.L. Belanovich, V.P. Savenko, A.I. Kulak, Plasma electrolytic ceramic-like aluminum oxide coatings on iron, J. Appl. Electrochem. 40 (2) (2010) 365–374, https://doi.org/10.1007/s10800-009-0005-1.

[12] T.W. Clyne, S.C. Troughton, A review of recent work on discharge characteristics during plasma electrolytic oxidation of various metals, Int. Mater. Rev. 64 (3) (2019) 127–162, https://doi.org/10.1080/09506608.2018.1466492.

[13] D.-S. Tsai, C.-C. Chou, Review of the soft sparking issues in plasma electrolytic oxidation, Materials 8 (2018) 105, https://doi.org/10.3390/met8020105.

[14] A.L. Yerokhin, V.V. Lyubimov, R.V. Ashitkov, Phase formation in ceramic coatings during plasma electrolytic oxidation of aluminium alloys, Ceram. Int. 24 (1998) 1–6, https://doi.org/10.1016/S0272-8842(96)00067-3.

[15] H. Sharift, M. Aliofkhazraei, G.B. Darband, A review on adhesion strength of PEO coatings by scratch test method, Surf. Rev. Lett. 25 (03) (2018) 1830004, https://doi.org/10.1142/S0218625X18300046.

[16] R.O. Hussein, D.O. Northwood, Production of anti-corrosion coatings on light alloys (Al, Mg, Ti) by plasma-electrolytic oxidation (PEO) (chapter 11), 2014, 202–238. http://doi.org/10.5772/57171.

[17] L.R. Krishna, K.R.C. Somaraju, G. Sundararajan, The tribological performance of ultrahard ceramic composite coatings obtained through micro-arc oxidation, Surf. Coat. Technol. 163–164 (2003) 484–490, https://doi.org/10.1016/S0257-8972(02)00646-1.

[18] L.R. Krishna, A.S. Purnima, G. Sundararajan, A comparative study of tribological behavior of micro-arc oxidation and hard-anodized coatings, Wear 261 (2006) 1095–1101, https://doi.org/10.1016/j.wear.2006.02.002.

[19] L. Shao, H. Li, B. Jiang, C. Liu, X. Gu, D. Chen, A comparative study of corrosion behavior of hard anodized and micro-arc oxidation coatings on 7050 aluminum alloy, Metals 8 (2018) 165, https://doi.org/10.3390/met8030165.

[20] A. Buling, J. Zerrer, Increasing the application fields of magnesium by ultraceramic: Corrosion and wear protection by plasma electrolytical oxidation (PEO) of Mg alloys, Surf. Coat. Technol. 369 (2019) 142–155, https://doi.org/10.1016/j.surfcoat.2019.04.025.

[21] X. Lu, Y. Chen, C. Blawert, Y. Li, T. Zhang, F. Wang, K.U. Kainer, M. Zheludkevich, Influence of SiO_2 particles on the corrosion and wear resistance of plasma electrolytic oxidation-coated AM50 Mg alloy, Coatings 8 (9) (2018) 306, https://doi.org/10.3390/coatings8090306.

[22] A.G. Rakoch, A.A. Gladkova, V.L. Kovalev, A.G. Seferyan, The mechanism of formation of composite microarc coatings on aluminum alloys, Prot. Met. Phys. Chem. Surf. 49 (7) (2013) 880–884, https://doi.org/10.1134/S2070205113070125.

[23] A.C. Bouali, E.A. Straumal, M. Serdechnova, D.C.F. Wieland, M. Starykevich, C. Blawert, J.U. Hammel, S.A. Lermontov, M.G.S. Ferreira, M.L. Zheludkevich, Layered double hydroxide based active corrosion protective sealing of plasma electrolytic oxidation/sol-gel composite coating on AA2024, Appl. Surf. Sci. 494 (2019) 829–840, https://doi.org/10.1016/j.apsusc.2019.07.117.

[24] A. Krząkała, A. Kazek-Kęsik, W. Simka, Application of plasma electrolytic oxidation to bioactive surface formation on titanium and its alloys, RSC Adv. 3 (43) (2013) 19725–19743, https://doi.org/10.1039/c3ra43465f.

[25] S. Stojadinović, N. Tadić, R. Vasilić, Formation and characterization of ZnO films on zinc substrate by plasma electrolytic oxidation, Surf. Coat. Technol. 307 (Part A) (2016) 650–657, https://doi.org/10.1016/j.surfcoat.2016.09.080.

[26] L. Grigorjeva, D. Millers, K. Smits, A. Zolotarjovs, Gas sensitive luminescence of ZnO coatings obtained by plazmaelectrolytic oxidation, Sens. Actuat., A 234 (2015) 290–293, https://doi.org/10.1016/j.sna.2015.09.018.

[27] E. Rocca, D. Veys-Renaux, K. Guessoum, Electrochemical behavior of zinc in KOH media at high voltage: micro-arc oxidation of zinc, J. Electroanal. Chem. 754 (2015) 125–132, https://doi.org/10.1016/j.jelechem.2015.06.021.

[28] P.A.I. Popoola, N. Malatji, O.S. Fayomi, Fabrication and properties of zinc composite coatings for mitigation of corrosion in coastal and marine zone (Chapter 7), 2016, pp. 1–29. http://doi.org/10.5772/62205.

[29] D. Crotty, Zinc alloy plating for the automotive industry, Met. Finish. 94 (9) (1996) 54–58, https://doi.org/10.1016/0026-0576(96)82103-9.

[30] S.W.K. Morgan, Zinc and its alloys and compounds, Ellis Horwood limited (1985).

[31] S. Battistona, C. Rigoa, E. da Cruz Severoa, M.A. Mazuttia, R.C. Kuhna, A. Gündelb, E.L. Foletto, Synthesis of zinc aluminate ($ZnAl_2O_4$) spinel and its application as photocatalyst, Mat. Res. 17 (3) (2014) 734–738, https://doi.org/10.1590/S1516-14392014005000073.

[32] E. Mostaed, M. Sikora-Jasinska, M. Vedani, Zinc-based degradable implants, Encyclopedia Biomed. Eng. (2019) 478–487, https://doi.org/10.1016/B978-0-12-801238-3.11022-0.

[33] E. Iruin, A.R. Mainar, M. Enterrí, N. Ortiz-Vitoriano, J.A. Blázquez, L.C. Colmenares, T. Rojo, S. Clark, B. Horstmann, Designing a manganese oxide bifunctional air electrode for aqueous chloride-based electrolytes in secondary zinc-air batteries, Electrochim. Acta 320 (2019) 134557, , https://doi.org/10.1016/j.electacta.2019.134557.

[34] J.A. Curran, T.W. Clyne, Porosity in plasma electrolytic oxide coatings, Acta Materialia 54 (2006) 1985–1993, https://doi.org/10.1016/j.actamat.2005.12.029.

[35] A. Yerokhin, L. Snizhko, N. Gurevina, A. Leyland, A. Pilkington, A. Matthews, Discharge characterization in plasma electrolytic oxidation of aluminium, J. Phys. D Appl. Phys. 36 (17) (2003) 2110.

[36] H. Dong, Surface engineering of light alloys, chapters 5 and 6, 110-180, Woodhead Publishing Limited, 2010, p. 680 p.

[37] E. Erfanifar, M. Aliofkhazraei, H. Fakhr, N. Hossein, S. Alireza, S. Rouhaghdam, Growth kinetics and morphology of plasma electrolytic oxidation coating on aluminum, Mater. Chem. Phys. 185 (2017) 162–175, https://doi.org/10.1016/j.matchemphys.2016.10.019.

[38] R.O. Hussein, X. Nie, D.O. Northwood, A. Yerokhin, A. Matthews, Spectroscopic study of electrolytic plasma and discharging behaviour during the plasma electrolytic oxidation (PEO) process, J. Phys. D Appl. Phys. 43 (2010) 105202, , https://doi.org/10.1088/0022-3727/43/10/105203.

[39] X. Yang, L. Chen, Y. Qu, R. Liu, K. Wei, W. Xue, Optical emission spectroscopy of plasma electrolytic oxidation process on 7075 aluminum alloy, Surf. Coat. Technol. 324 (2017) 18–25, https://doi.org/10.1016/j.surfcoat.2017.05.005.

[40] L. Wang, L. Chen, Z. Yan, Wen Fu, Optical emission spectroscopy studies of discharge mechanism and plasmacharacteristics during plasma electrolytic oxidation of magnesium indifferent electrolytes, Surf. Coat. Technol. 205 (2010) 1651–1658, https://doi.org/10.1016/j.surfcoat.2010.10.022.

[41] R. Arrabal, E. Matykina, T. Hashimoto, P. Skeldon, G.E. Thompson, Characterization of AC PEO coatings on magnesium alloys, Surf. Coat. Technol. 203 (2009) 2207–2220, https://doi.org/10.1016/j.surfcoat.2009.02.011.

[42] M.D. Klapkiv, H.M. Nykyforchyn, V.M. Posuvailo, Spectral analysis of an electrolytic plasma in the process of synthesis of aluminum oxide, Mater. Sci. 30 (1994) 333, https://doi.org/10.1007/BF00569685.

[43] V. Dehnavi, X.Y. Liu, B.L. Luan, D.W. Shoesmith, S. Rohani, Phase transformation in plasma electrolytic oxidation coatings on 6061 aluminum alloy, Surf. Coat. Technol. 251 (2014) 106–114, https://doi.org/10.1016/j.surfcoat.2014.04.010.

[44] S. Stojadinović, N. Tadić, N. Radić, B. Stojadinovic, B. Grbić, R. Vasilic, Synthesis and characterization of Al_2O_3/ZnO coatings formed by plasma electrolytic oxidation, Surf. Coat. Technol. 276 (2015) 573–579, https://doi.org/10.1016/j.surfcoat.2015.06.013.

[45] S. Stojadinović, R. Vasilić, Spectroscopic study of micro-discharges during plasma electrolytic oxidation of Al–Zn–Si alloy, J. Serb. Chem. Soc. 84 (2019) 915–923, https://doi.org/10.2298/JSC190418040S.

[46] N.J. van der Laag, M.D. Snel, Pieter C.M.M. Magus, Pieter C.M.M. Magusin, G. de With, Structural, elastic, thermophysical and dielectric properties of zinc aluminate ($ZnAl_2O_4$), J. Europ. Ceram. Soc. 24 (8) (2004) 2417–2424, https://doi.org/10.1016/j.jeurceramsoc.2003.06.001.

[47] A.S. Shaporeva, V.K. Ivanova, A.E. Baranchikova, O.S. Polezhaeva, Yu. D. Tret'yakov, ZnO formation under hydrothermal conditions from zinc hydroxide compounds with various, Chem. Histories, Russian J. Inorg. Chem. 52 (12) (2007) 1811–1816, https://doi.org/10.1134/S0036023607120017.

[48] B. Zhang, X. Li, D. Li, Assessment of thermal expansion coefficient for pure metals, Calphad 43 (2013) 7–17, https://doi.org/10.1016/j.calphad.2013.08.006.

[49] M. Singh, M. Singh, Thermal expansion in zinc oxide nanomaterials, Nanosci. Nanotechn. Res. 1 (2) (2013) 27–29, https://doi.org/10.12691/nnr-1-2-4.

[50] S.M. Buchi, J. Roy, Synthesis and high temperature dielectric and complex impedance spectroscopic studies of dense $ZnAl_2O_4$ ceramics, Mater. Sci. Eng. J. 1 (1) (2017) 1001.

[51] P.S. Sokolov, A.N. Baranov, A.M.T. Bell, V.L. Solozhenko, Low-temperature thermal expansion of rock-salt ZnO, Solid State Comm. 177 (2014) 65–67, https://doi.org/10.1016/j.ssc.2013.10.006.